EERI EARTHQUAKE SPECTRA

A seismologically consistent surface rupture length model for unbounded and width-limited events

Grigorios Lavrentiadis, M.EERI[1,2] (iD),
Yonfei Wang, M.EERI[3]**, Norman A Abrahamson,
M.EERI**[4]**, Yousef Bozorgnia, M.EERI**[2] (iD)**, and
Christine A Goulet, M.EERI**[5] (iD)

Abstract

A new surface-rupture-length (SRL) relationship as a function of magnitude ($\mathbf{M}$), fault thickness, and fault dip angle is presented in this article. The objective of this study is to model the change in scaling between unbounded and width-limited ruptures. This is achieved through the use of seismological-theory-based relationships for the average displacement scaling and the aid of dynamic fault rupture simulations to constrain the rupture width scaling. The empirical data set used in the development of this relationship is composed of 122 events ranging from $\mathbf{M}$ 5 to 8.1 and SRL 1.1 to 432 km. The dynamic rupture simulations data set includes 554 events ranging from $\mathbf{M}$ 4.9 to 8.2 and SRL 1 to 655 km. For the average displacement ($\bar{D}$) scaling, three simple models and two composite models were evaluated. The simple average displacement models are a square root of the rupture area ($\sqrt{A}$), a down-dip width (W), and a rupture length (L) proportional model. The two composite models have a $\sqrt{A}$ scaling for unbounded ruptures and transition to W and L scaling for width-limited events, respectively. The empirical data favors a $\bar{D} \sim \sqrt{A}$ scaling for the entire regime (unbounded and width-limited ruptures) followed by a $\sqrt{A}$ scaling for unbounded that changes to L scaling for width-limited ruptures. The selected models exhibit better predictive performance compared to linear $\log(\mathrm{SRL}) \sim \mathbf{M}$ type models, especially in the large magnitude range, which is dominated by width-limited events. A comparison with published SRL models shows consistent scaling for different fault types and tectonic environments.

[1]Department of Mechanical and Civil Engineering, California Institute of Technology, Pasadena, CA, USA
[2]Natural Hazards Risk and Resiliency Research Center (NHR3), University of California Los Angeles, Los Angeles, CA, USA
[3]Southern California Earthquake Center, University of Southern California, Los Angeles, CA, USA
[4]Department of Civil and Environmental Engineering, University of California, Berkeley, Berkeley, CA, USA
[5]Pasadena Field Office, U.S. Geological Survey, Pasadena, CA, USA

Corresponding author:
Grigorios Lavrentiadis, Department of Mechanical and Civil Engineering, California Institute of Technology, Pasadena, CA 91125, USA.
Email: glavrent@caltech.edu

Introduction

Surface-rupture fault displacement hazard analyses, both probabilistic and deterministic, require an estimate of the surface rupture length (SRL) to compute the shape of the slip profile (Lavrentiadis and Abrahamson, 2019; Moss and Ross, 2011; Petersen et al., 2011; Youngs et al., 2003). Studies such as Wells and Coppersmith (1994), Wesnousky (2008), and Wells and Youngs (2015) proposed empirical models for the SRL scaling using observations from past earthquakes. These models are straightforward to develop and have good predictive performances within the range of data, but they may exhibit poor extrapolation for large events as the mechanisms that control the SRL scaling in large earthquakes, which are not well understood due to the scant empirical data. Another approach for developing scaling relationships is based on the use of theoretical considerations and constraints. Examples of such models are Leonard (2010, 2014), who developed sets of equations that describe the scaling between seismic moment, rupture area, length, width, and average displacement by imposing a self-consistent constraint. This type of theory-based model may have slightly larger aleatory variability at the center of the data compared to the purely empirical models, due to the incorporation of seismological constraints, but exhibit better extrapolation behavior.

The impact of the thickness of the seismogenic zone in the geometry of the rupture has been observed by previous studies, for instance, Hanks and Bakun (2002) proposed a magnitude break in their $\log(A) \sim \mathbf{M}$ relationship at magnitude $\mathbf{M} = 6.71$, while Leonard (2014) proposed bi-linear and tri-linear relationships for $\mathbf{M} \sim \log(L)$ and $\mathbf{M} \sim \log(SRL)$ relationships, depending on the style of faulting and tectonic environment. However, to the authors' knowledge, a relationship that explicitly considers the effect of the finite seismogenic zone thickness in the $\log(SRL) \sim \mathbf{M}$ scaling does not exist. The recent development of extensively documented community-based fault displacement databases and advances in computer-based earthquake rupture simulation methods (both described below) motivated the development of the model presented herein, which explores this issue. The objective of this study is to develop a new SRL relationship that captures the changes in scaling between unbounded and width-limited ruptures. The impact of the change in scaling is expected to be more pronounced in active crustal regions (ACRs) with thin seismogenic zones, such as California, as opposed to stable continental regions with thicker seismogenic zones, such as Australia or the northeastern part of the North American continent.

A sketch illustrating the two conditions is presented in Figure 1. Assuming a similar static stress drop between the two regions, events of similar magnitude are expected to have similar rupture areas (A) (Equation 1 from Brune, 1971). In addition, making the assumption that ruptures grow with similar aspect ratio scaling, small events that produce surface rupture, which do not reach the bottom of the seismogenic zone, are expected to have similar rupture geometries (rupture length and width), between the two regions. However; for moderate-to-large events, the thinner seismogenic zone is expected to impede the growth of the rupture width at shallower depths, requiring the rupture length to grow faster in order
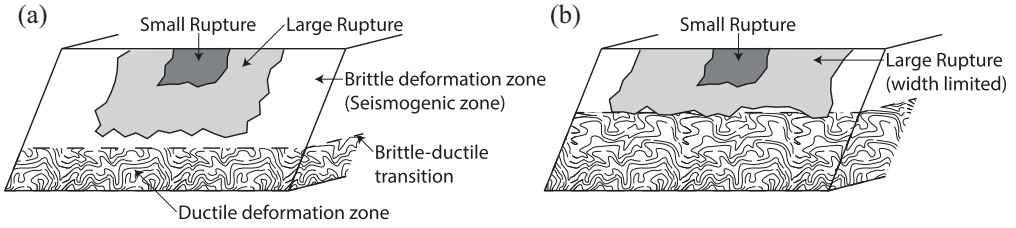
Figure 1. Sketches of rupture geometries for small (dark shading) and moderate-to-large (pale shading) events (a) in thick crust regions and (b) in thin crust regions.

to accommodate the same rupture area, which will result in a magnitude break and steeper scaling for SRL.

$$\log(M_o) = 3/2\log(A) + \log(\Delta\sigma) - 0.387 \tag{1}$$

In the following sections, the term "unbounded rupture" is used to classify the ruptures of the events not limited by the width of the seismogenic zone, and the term "width-limited ruptures" is used to classify the ruptures of the events that are constrained by the finite width of the seismogenic zone.

Data

Two sets of data were used in developing the proposed model: an empirical data set used for the SRL scaling (Subsection: Empirical Data) and a numerical physics-based simulation data set used to constrain the rupture width scaling (Subsection: SCEC Simulations). The empirical and numerical simulation data sets can be accessed from the repositories provided in the Subsection: Data and Resources.

Empirical data

The empirical data sets used in the model development include: (i) the Fault Displacement Hazard Initiative (FDHI) data set (Sarmiento et al., 2022), (ii) additional events from Wells and Coppersmith (1994), which they classified as reliable, and (iii) the surface rupture events from Baize et al. (2020) which were not part of the FDHI data set. Events less than **M**5 were excluded from the final data set, as well as the 1892 Laguna Salada, 1978 IzuOshima, and 1993 Killari earthquakes which were considered outliers. Potential reasons for considering the previous events as outliers are the Laguna Saldana earthquake ruptured in the 1800s but was mapped in the 2010s, so large parts of the rupture may have been irrecoverable; the 1978 Izu Oshima earthquake likely included an offshore segment that was not mapped in the FDHI data set; and the 1993 Killari occurred in a stable continental region with a lot of deformation probably accommodated via folding/warping that was unmapped.

The SRL values for the events from Wells and Coppersmith (1994) and Baize et al. (2020) were obtained directly from the corresponding studies, while for the events in the FDHI data set, SRL was estimated based on the length of the event coordinate system (ECS) defined in Lavrentiadis and Abrahamson (this issue). ECS's goal is to define the along-strike and perpendicular-to-strike distance metrics for the FDHI events whose

points are georeferenced on the latitude and longitude coordinates. Comparisons of the SLR reported by Wells and Coppersmith (1994) and Baize et al. (2020) with those obtained from ECS showed unbiased consistent estimates. Figure 2 shows the SRL versus **M** distribution of the final empirical data set. It is composed of 64 events from FDHI, 52 events from Wells and Coppersmith (1994), and 6 events from Baize et al. (2020). The earthquake **M** ranges from 5.0 to 8.1, while SRL ranges from 1.1 to 432 km. It contains 64 strike-slip, 26 normal, and 32 reverse earthquakes.

The fault width ($W_{\lim}$) required to define the transition to a width-limited rupture was estimated with Equation 2 based on the thickness of the seismogenic zone (D_{seis}) and the fault dip angle (θ). D_{seis} was based on the fault location, as summarized in Table 1, whereas θ was based on the style of faulting, as summarized in Table 2. In the absence of fault-specific information, representative D_{seis} and θ values were obtained from Huang et al. (2023), while the number of events belonging to each region is also summarized in Table 1.

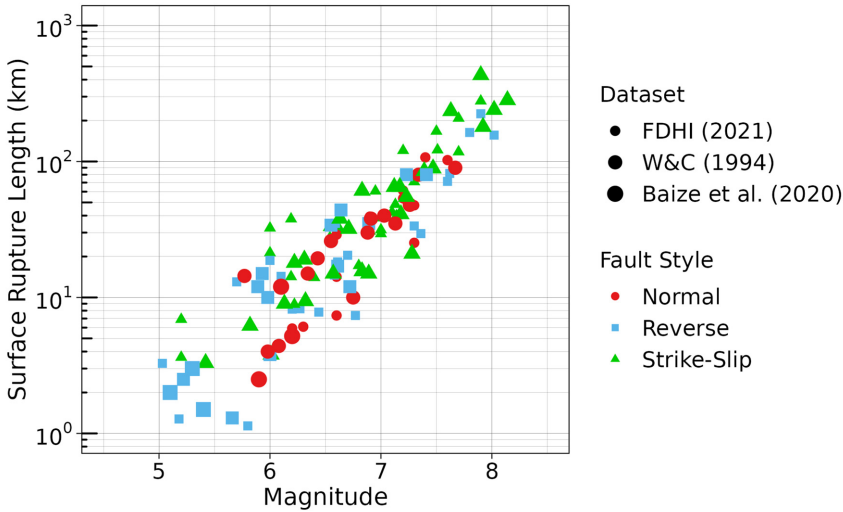$$W_{\lim} = \frac{D_{seis}}{\sin(\theta)} \qquad (2)$$

Figure 2. Comparison of Magnitude **M**–Surface Rupture Length (SRL) distribution of empirical data sets.

Table 1. Seismogenic thickness and number of events of different regions

Region	Seismogenic thickness (km)	Number of events
California	15	29
Guatemala	15	1
New Zealand	15	3
Indonesia	15	1
Japan	17	7
Himalayan region	30	12
Australia	40	11
Other regions	22	57

Table 2. Dip angle values for different styles of faulting

Style of faulting	Dip angle (deg)
Strike-slip	90
Normal	60
Reverse	45

Dynamic rupture simulations

The data set used for constraining the rupture width scaling is based on physics-based fault displacement simulations conducted by the Southern California Earthquake Center (SCEC) as part of the FDHI efforts. The physics-based approach used in this study is referred to as the dynamic rupture model (Harris et al., 2018); it constructs spontaneously evolving earthquake ruptures under mechanical causative conditions (e.g., fault geometry, friction laws, stress conditions, and surrounding rock properties). Figure 3 illustrates a simplified workflow of the dynamic rupture model. To simulate realistic fault displacement, we follow the methodology (Wang and Goulet, 2021) originated from the 1992 Landers earthquake. We adopt a depth-dependent lithostatic load for vertical stress and self-similarly heterogeneous shear stress that permits unprescribed variability in rupture
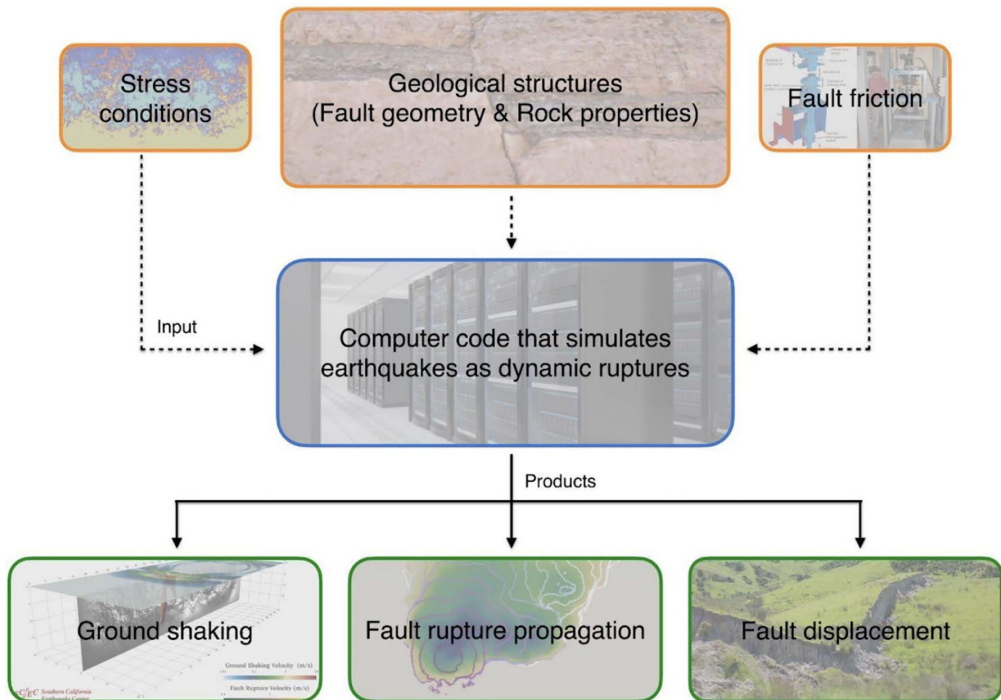

Figure 3. Key ingredients and schematic pipeline of a dynamic earthquake rupture simulation. Inputs include the initial stress conditions, the fault structure, the properties of the nearby rocks, and formulations that describe how the fault slips. A computer program numerically solves the resultant fault rupture propagation and wave propagation and outputs the ground shaking and fault displacements.

style and size. With regard to the friction law, we similarly select the slip-weakening law (Ida, 1972). In contrast to the general theoretical considerations such as those used by Leonard (2010), the dynamic rupture model employs a physically plausible parametric uncertainty (i.e., heterogeneous initial stress) to capture the displacement variability across the rupture plane due to the elasto-plasto-dynamic response to imposed stresses. The SRL is then computed using numerical criteria. For the purpose of this article, the length is represented by summing the length of fault segments with surface displacement larger than 1 cm.

The fault displacements were simulated by numerically solving the 3D elastoplastic spontaneous rupture propagation with the Support Operator Rupture Dynamics (SORD) code (Wang and Day, 2017, 2020; Wang and Goulet, 2021). This application is highly optimized and scalable on current cutting-edge supercomputers. This is a requirement since to capture a **M** range of 5–8 associated with rupture lengths of several kilometers to hundreds of kilometers, the computational demands vary from seconds on tens of CPUs to hours on hundreds of thousands of CPUs. The simulations described here were performed on Theta at the Argonne Leadership Computing Facility and Frontera at the Texas Advanced Computing Center.

A series of dynamic fault rupture simulations under various model setups were therefore performed to understand and model the effect of fault width in the SRL scaling. The general parameters were set based on the work of Wang and Goulet (2021), with additional variations, as described below, all for vertical strike-slip faults. One set of simulations was performed in which the fault width was limited to 19 km, with two variations in the normal loading stresses pattern: fixed with depth in one case, and linearly increasing with depth in the other. The other set of simulations involved limiting the fault width to 15 km while maintaining the other model parameters fixed. It is noted that although a width limit is provided for the dynamic rupture models (15 and 19 km), the resultant ruptures, which are generated based on the initial conditions and physical laws, are not prescribed, which results in the scattered characteristics shown in Figures 4 and 5. The simulations output includes determining the moment mangitude (**M**), which is not a priori imposed, the rupture geometry, and the displacement field across the fault plane. The simulations were continued to generate a wavefield and to provide surface ground motions, which were verified against existing ground motion models (GMMs), to ensure that the simulations were reasonable and technically defensible. A detailed description of the dynamic rupture model can be found in Wang and Goulet (2022).

In total, 554 simulations were performed with magnitude ranging from 4.9 to 8.2 and SRL ranging from 1 to 655 km. Figure 4 compares the $\mathbf{M} - SRL$ scaling of the empirical and SCEC data sets. Overall, the empirical and simulation data sets appear consistent, supporting the use of the simulation data sets to inform the mean SRL scaling in the empirical data. The aleatory variability of the SCEC data set is expected to be less than that of the empirical data, as the goal of the simulations was to capture average scaling effects and not to fully represent the randomness and uncertainty in earthquake ruptures.

Model development

The derivation of the SRL model is divided into two parts. In the first part, an average model for the rupture width (W) scaling of unbounded and width-limited ruptures based on the SCEC simulations is proposed. In the second part, the SRL model based on the
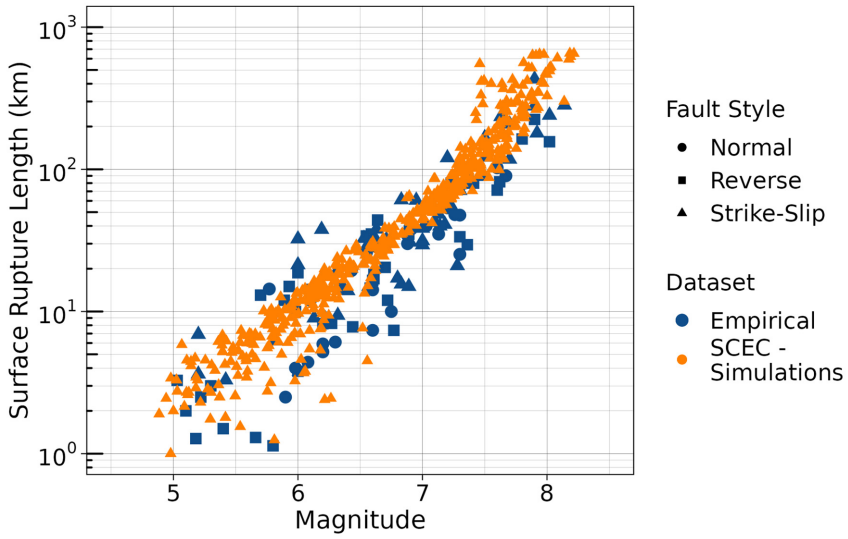
Figure 4. Comparison of magnitude–surface rupture length (SRL) distribution of empirical data sets and SCEC simulations.
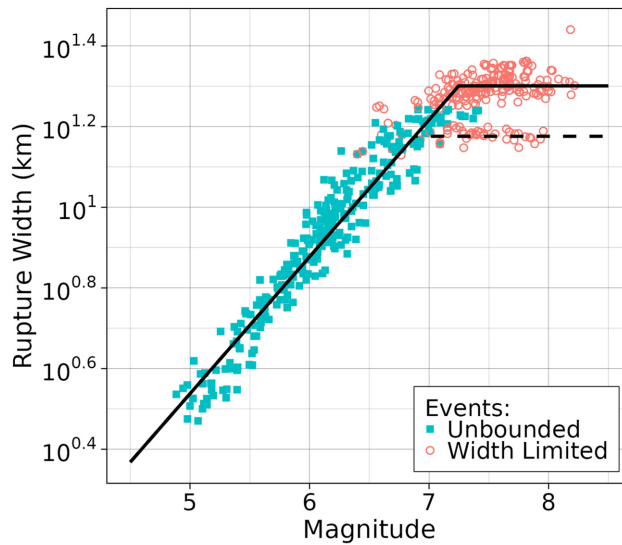

Figure 5. Comparison of magnitude–rupture width model with SCEC simulations. The solid vertical line corresponds to a 19 km fault width, dashed vertical line corresponds to a 15 km fault width.

empirical data is developed with the aid of the W model to capture the transition between unbounded and width-limited ruptures.

Rupture width modeling

Although the physics-based simulations have complete slip profiles on fault planes, the rupture widths are sensitive to where rupture arrest may be subjectively measured. To

Table 3. Rupture width model coefficients

Coefficient	β_1	β_2	σ_W
Estimate	-1.1602	0.3395	0.0544
Standard error	0.0325	0.0053	—

avoid this, we adopt the approach originally developed for extracting rupture widths from finite fault models by Mai and Beroza (2000) to define the effective rupture width (the autocorrelation width of depth-variable slip profile) and apply this method to all simulation-based data sets for rupture width measurements. Then, the effective rupture widths, estimated from the SCEC simulations, were used to determine the width scaling relationship. A linear functional form with a plateau for the upper limit is proposed:

$$\log_{10}(W) = \min(\beta_1 + \beta_2 \mathbf{M} + \epsilon_W, \, \log_{10}(W_{\lim})) \tag{3}$$

in which the log of the rupture width scales linearly with magnitude until it reaches the fault width, where it remains constant. The coefficient β_1 is the model intercept, β_2 controls the magnitude scaling, and ϵ_W is the aleatory term that is modeled with a normal distribution with a zero mean and σ_W standard deviation ($\epsilon_W \sim \mathcal{N}(0, \sigma_W)$) The model coefficients were estimated with a linear regression; the best estimates and standard error values of the model coefficients are provided in Table 3. In the SCEC simulations, events were classified as width-limited if the effective width was within ± 2.5 km of the prescribed maximum width. Figure 5 compares the scaling of the proposed model with the SCEC simulations, and Figure 6 presents the regression residuals, where it can be seen that there is a small misfit in the different magnitude bins, but overall, the model captures the fundamental scaling of the SCEC simulations and the transition between unbounded and width-limited ruptures. A tri-linear relationship is expected to improve the fit; however, it will also introduce additional complexity, which cannot be adequately characterized with the limited number of simulations; for this reason, the simpler bi-linear model was selected. In addition, any simplifications or differences in the width scaling between the SCEC simulations and empirical data will be mapped into the aleatory variability of the SRL model described in the next section.

SRL modeling

In developing the SRL model, the candidate functional forms are derived in Section: Functional Form Derivation, and the model coefficients are estimated in Section: Functional Form Derivation along with a discussion on the selection of the preferred and alternative models.

Functional form derivation. Starting with the definition of the seismic moment ($M_0 = \mu \bar{D} L W$), and substituting it into the definition of the moment magnitude ($\mathbf{M} = 2/3 \log_{10}(M_0) - 10.7$), (Kanamori, 1977), a relationship between $\mathbf{M}$, average rupture slip ($\bar{D}$), subsurface rupture length (L), subsurface rupture width (W), and crust stiffness (μ) is obtained:

$$\mathbf{M} = \frac{2}{3}\log_{10}(\mu) + \frac{2}{3}\log_{10}(\bar{D}) + \frac{2}{3}\log_{10}(L) + \frac{2}{3}\log_{10}(W) - 10.7 \tag{4}$$
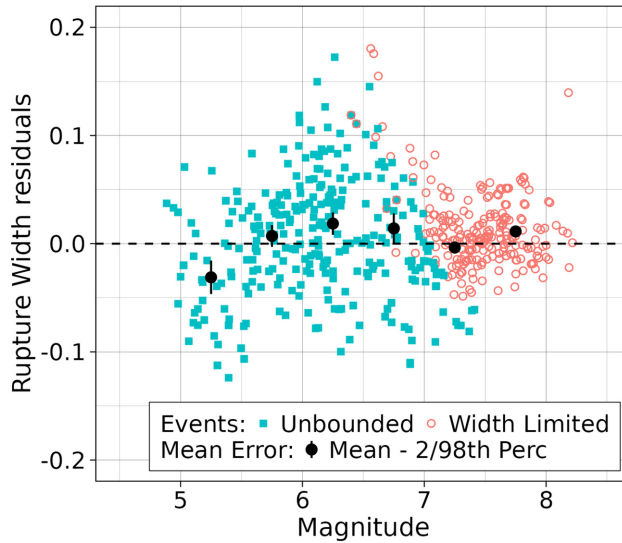
Figure 6. Residuals of magnitude–rupture width model with the SCEC simulations. The solid circles correspond to the bias of the residuals, while the tips of the vertical bars correspond to the 2nd and 98th percentile of the standard error of the mean.

Treating μ as model constant and combining it with the -10.7 factor, the previous equation reduces to:

$$\mathbf{M} = \frac{2}{3} \log_{10}(\bar{D}) + \frac{2}{3} \log_{10}(L) + \frac{2}{3} \log_{10}(W) + c \tag{5}$$

Here and in the remainder of this article, c with no subscript is used to indicate any arbitrary constant, not a specific model coefficient.

Two end-member scaling relationships for average displacement often discussed in the literature (Bodin and Brune, 1996; Hanks and Bakun, 2002; Leonard, 2010; Pegler and Das, 1996; Romanowicz, 1992, 1994; Romanowicz and Rundle, 1993; Scholz, 1982, 1994, 1997, 1998) are the L model, in which average displacement is proportional to rupture length ($\bar{D} \sim L$), and the W model, in which average displacement is proportional to rupture width ($\bar{D} \sim W$). More recent studies suggest that slip scaling is between L and W models (Bodin and Brune, 1996; Mai and Beroza, 2000). Leonard (2010) proposed the $\bar{D} \sim \sqrt{A}$ model, in which the average displacement scales proportionally to the square root of the rupture area. Here, we investigated all three scaling relationships in building the SRL$\sim$**M** model, as well as two composite scaling laws that follow $\bar{D} \sim \sqrt{A}$ for the unbounded ruptures and transition to $\bar{D} \sim L$ and $\bar{D} \sim W$ for width-limited events, respectively. In particular, the SRL relationship based on $\bar{D} \sim \sqrt{A}$ scaling is denoted model 1, the relationship based on $\bar{D} \sim W$ scaling is denoted model 2, and the relationship based on $\bar{D} \sim L$ scaling is denoted model 3. The scaling relationship that starts with $\bar{D} \sim \sqrt{A}$ and transitions to $\bar{D} \sim W$ is denoted model 2′ while the scaling relationship that transitions to $\bar{D} \sim L$ is denoted model 3′.

By substituting the $\bar{D} \sim \sqrt{A}$ scaling in Equation 5, the following scaling relationship between $\mathbf{M}$, L, and W is obtained for model 1:

$$\mathbf{M} = \log_{10}(L) + \log_{10}(W) + c \tag{6}$$

Combining Equation 5 with the $\bar{D} \sim W$ scaling, the model 2 scaling relationship becomes:

$$\mathbf{M} = \frac{2}{3}\log_{10}(L) + \frac{4}{3}\log_{10}(W) + c \tag{7}$$

While, combining Equation 5 with the $\bar{D} \sim L$ model, the model 3 scaling relationship becomes:

$$\mathbf{M} = \frac{4}{3}\log_{10}(L) + \frac{2}{3}\log_{10}(W) + c \tag{8}$$

Adopting the rupture width scaling relationship from Section: Rupture Width Modeling assuming the surface to subsurface rupture length relationship is of the form: $\log_{10}(\mathrm{SRL}) = c_1 \log_{10}(L) + c$ (Leonard, 2010), and solving for $\log_{10}(\mathrm{SRL})$, model 1 transforms to:

$$\log_{10}(\mathrm{SRL}) = c_1(\mathbf{M} - \min(\beta_1 + \beta_2\mathbf{M}, \log_{10}(W_{\mathrm{lim}}))) + c \tag{9}$$

model 2 transforms to:

$$\log_{10}(\mathrm{SRL}) = c_1\left(\frac{3}{2}\mathbf{M} - 2\min(\beta_1 + \beta_2\mathbf{M}, \log_{10}(W_{\mathrm{lim}}))\right) + c \tag{10}$$

and model 3 transforms to:

$$\log_{10}(\mathrm{SRL}) = c_1\left(\frac{3}{4}\mathbf{M} - \frac{1}{2}\min(\beta_1 + \beta_2\mathbf{M}, \log_{10}(W_{\mathrm{lim}}))\right) + c \tag{11}$$

Considering Equations 9 and 10, the functional form the composite model $2'$ is:

$$\log_{10}(\mathrm{SRL}) = \begin{cases} c_1(\mathbf{M} - \min(\beta_1 + \beta_2\mathbf{M}, \log_{10}(W_{\mathrm{lim}})) + d_1) + c & \mathbf{M} \leqslant \mathbf{M}_{\mathrm{lim}} \\ c_1\left(\frac{3}{2}\mathbf{M} - 2\min(\beta_1 + \beta_2\mathbf{M}, \log_{10}(W_{\mathrm{lim}}))\right) + c & \mathbf{M} > \mathbf{M}_{\mathrm{lim}} \end{cases} \tag{12}$$

where $\mathbf{M}_{\mathrm{lim}}$ is the magnitude at which the transition from unbounded to width-limited events occurs. The term d_1 is introduced to ensure a continuous transition between the two branches. Using Equation 3, $\mathbf{M}_{\mathrm{lim}}$ is calculated as: $\mathbf{M}_{\mathrm{lim}} = 1/\beta_2(\log_{10}(W_{\mathrm{lim}}) - \beta_1)$. The transition from unbounded to width-limited events occurs at the $(\mathbf{M}_{\mathrm{lim}}, W_{\mathrm{lim}})$ coordinate pair. Setting the two branches equal to each other at the transition point and solving for d_1, we obtain:

$$d_1 = -\frac{1}{2}\mathbf{M}_{\mathrm{lim}} + \log_{10}(W_{\mathrm{lim}}) \tag{13}$$

With the previous equation, the two branches of model 2′ are combined into one equation:

$$\log_{10}(\text{SRL}) = c_1\left(\frac{3}{2}\mathbf{M} - \frac{1}{2}\min(\mathbf{M}, \mathbf{M}_{\text{lim}}) - \min(\beta_1 + \beta_2\mathbf{M}, \log_{10}(W_{\text{lim}}))\right) + c \qquad (14)$$

Similarly, considering Equations 9 and 11, the functional form of the composite model 3′ is:

$$\log_{10}(\text{SRL}) = \begin{cases} c_1(\mathbf{M} - \min(\beta_1 + \beta_2\mathbf{M}, \log_{10}(W_{\text{lim}})) + d_2) + c & \mathbf{M} \leqslant \mathbf{M}_{\text{lim}} \\ c_1\left(\frac{3}{4}\mathbf{M} - \frac{1}{2}\min(\beta_1 + \beta_2\mathbf{M}, \log_{10}(W_{\text{lim}}))\right) + c & \mathbf{M} > \mathbf{M}_{\text{lim}} \end{cases} \qquad (15)$$

Following a similar derivation to model 2′, the functional form of model 3′ can be expressed as:

$$\log_{10}(\text{SRL}) = c_1\left(\frac{3}{4}\mathbf{M} + \frac{1}{4}\min(\mathbf{M}, \mathbf{M}_{\text{lim}}) - \min(\beta_1 + \beta_2\mathbf{M}, \log_{10}(W_{\text{lim}}))\right) + c \qquad (16)$$

The style of faulting is implicitly included in the previous scaling relationships through W_{lim}; normal and reverse faults have shallower dip angles compared to strike-slip faults leading to larger fault widths for the same seismological zone thickness. However, an additive term for dip-slip faults (F_D) is also added in the final functional forms to account for differences in the static stress drop between the different styles of faulting. In preliminary regressions, separate additive terms for normal and reverse faults were also evaluated but were rejected to favor model simplicity as both reverse and normal faults had similar additive term values. The static stress drop is defined as:

$$\Delta\sigma = C\mu\frac{\bar{D}}{L_C} \qquad (17)$$

where L_C is the characteristic length, and C is a constant which is a function of the rupture geometry. In the log scale, a shift in the static stress drop will be accompanied by a shift in the average displacement ($\log(\bar{D}) = \log(\Delta\sigma) + c$), which, in turn, will shift the intercept of the SRL~$\mathbf{M}$ relationship. Thus, the final functional form for model 1 becomes:

$$\begin{aligned} \log_{10}(\text{SRL}) &= c_0 + c_1(\mathbf{M} - \min(\beta_1 + \beta_2\mathbf{M}, \log_{10}(W_{\text{lim}}))) + c_2 F_D + \epsilon_{\text{SRL}} \\ &= c_0 + c_1 X_1 + c_2 F_D + \epsilon_{\text{SRL}} \end{aligned} \qquad (18)$$

which can be expressed as a linear model with $X_1 = (\mathbf{M} - \min(\beta_1 + \beta_2\mathbf{M}, \log_{10}(W_{\text{lim}})))$. The functional form for model model 2′ is:

$$\begin{aligned} \log_{10}(\text{SRL}) &= c_0 + c_1\left(\frac{3}{2}\mathbf{M} - 2\min(\beta_1 + \beta_2\mathbf{M}, \log_{10}(W_{\text{lim}}))\right) + c_2 F_D + \epsilon_{\text{SRL}} \\ &= c_0 + c_1 X_2 + c_2 F_D + c_3 + \epsilon_{\text{SRL}} \end{aligned} \qquad (19)$$

with $X_2 = (3/2\mathbf{M} - 2\min(\beta_1 + \beta_2\mathbf{M}, \log_{10}(W_{\text{lim}})))$ to be expressed as a linear model. The functional form for model 3 is:

$$\log_{10}(\text{SRL}) = c_0 + c_1 \left(\frac{3}{4} \mathbf{M} - \frac{1}{2} \min(\beta_1 + \beta_2 \mathbf{M}, \log_{10}(W_{\lim})) \right) + c_2 F_D + \epsilon_{\text{SRL}}$$
$$= c_0 + c_1 X_3 + c_2 F_D + c_3 + \epsilon_{\text{SRL}} \tag{20}$$

with $X_3 = (3/4 \mathbf{M} - 1/2 \min(\beta_1 + \beta_2 \mathbf{M}, \log_{10}(W_{\lim})))$. Model 2′ final functional form is:

$$\log_{10}(\text{SRL}) = c_0 + c_1 \left(\frac{3}{2} \mathbf{M} - \frac{1}{2} \min(\mathbf{M}, \mathbf{M}_{\lim}) - \min(\beta_1 + \beta_2 \mathbf{M}, \log_{10}(W_{\lim})) \right)$$
$$+ c_2 F_D + \epsilon_{\text{SRL}}$$
$$= c_0 + c_1 X'_2 + c_2 F_D + c_3 + \epsilon_{\text{SRL}} \tag{21}$$

with $X'_2 = \left(\frac{3}{2} \mathbf{M} - \frac{1}{2} \min(\mathbf{M}, \mathbf{M}_{\lim}) - \min(\beta_1 + \beta_2 \mathbf{M}, \log_{10}(W_{\lim})) \right)$, and model 3′ final functional form is:

$$\log_{10}(\text{SRL}) = c_0 + c_1 \left(\frac{3}{4} \mathbf{M} + \frac{1}{4} \min(\mathbf{M}, \mathbf{M}_{\lim}) - \min(\beta_1 + \beta_2 \mathbf{M}, \log_{10}(W_{\lim})) \right)$$
$$+ c_2 F_D + \epsilon_{\text{SRL}}$$
$$c_0 + c_1 X'_3 + c_2 F_D + c_3 + \epsilon_{\text{SRL}} \tag{22}$$

with $X'_3 = \left(\frac{3}{4} \mathbf{M} + \frac{1}{4} \min(\mathbf{M}, \mathbf{M}_{\lim}) - \min(\beta_1 + \beta_2 \mathbf{M}, \log_{10}(W_{\lim})) \right)$.

Finally, a Wells and Coppersmith type model was also evaluated, hereafter referred to as model 0, to investigate the impact of width-limited ruptures on the current state of practice models. The functional form for model 0 is:

$$\log_{10}(\text{SRL}) = c_0 + c_1 \mathbf{M} + c_2 F_D + \epsilon_{\text{SRL}} \tag{23}$$

In all previous equations, c_0 is the model intercept, c_1 controls the magnitude scaling, c_2 captures the median shift between strike-slip and dip-slip events (F_D is zero for strike-slip and one for reverse and normal faults), and ϵ_{SRL} is the aleatory term. More information on the modeling of the aleatory variability is provided at the end of Subsection: Model Regression.

Model regression. All candidate models were estimated using a maximum likelihood linear regression and the empirical data set. Table 4 provides the log-likelihood ($\mathcal{L}$) and Akaike information criterion (AIC, Akaike, 1998) for the different models; a higher $\mathcal{L}$ and lower

Table 4. Log-likelihood ($\mathcal{L}$) and Akaike information criterion (AIC) of the candidate rupture length models

Model	$\mathcal{L}$	AIC
Model 0	6.06	−4.12
Model 1	15.42	−22.85
Model 2	14.15	−20.30
Model 3	14.30	−20.60
Model 2′	8.91	−9.81
Model 3′	12.22	−16.44

AIC indicate a better model fit to the data. Table 5 summarizes the best estimates and standard errors of the model coefficients.

From a statistical perspective, candidate models 1 to 3 have similar good performance, with model 1 having the best performance. Models 3′ and model 2′ which have poorer performance, while model 0 has the worst performance showcasing the limitations of a purely empirical model. Models 1 to 3′ have a break in the magnitude scaling when the width of the rupture reaches the width of the seismogenic zone, allowing them to fit the data better.

However, based on seismological theory, models 1 to 3′ should also have unit slopes with respect to the magnitude scaling terms (e.g., X_1, X_2, X_3), if the average displacement in the empirical data follows the assumed scaling law and the subsurface rupture length (L) was the response variable. With SRL being the response variable, a magnitude scaling term greater than unity implies that the surface-to-subsurface rupture length ratio increases with magnitude, while a magnitude scaling term less than unity implies the opposite. Intuitively, a larger than one magnitude scaling term is expected, as for large events, a bigger part of the rupture is expected to reach the surface. Considering that model 1 exhibited the best predictive performance, but the magnitude scaling term was slightly less than one, the final preferred model uses model 1 functional form (Equation 18) with a fixed unit slope. Similarly, model 3′ has a slope consistent with seismological theory and decent predictive performance; thus, model 3′ with a fixed unit slope (Equation 21) is selected as an alternative physically plausible model. The statistical measures for the goodness of fit and coefficients of the preferred and alternative models are summarized in Tables 6 and 7, respectively.

The findings of the regression analyses favor a $\sim\sqrt{A}$ scaling for the entire regime or a $\sim\sqrt{A}$ scaling that transitions to a $\sim\sqrt{L}$ scaling for width-limited events for the average displacement compared to a pure $\sim W$ and $\sim L$ scaling or a $\sim\sqrt{A}$ scaling that transitions

Table 5. Rupture length candidate model coefficients

Model	Coefficient	c_0	c_1	c_2	$\sigma_{SRL-unb}$
Model 0	Estimate	2.9680	0.6629	−0.1836	0.2331
	Standard error	0.2126	0.0305	0.0484	−
Model 1	Estimate	−3.8783	0.9509	−0.1517	0.2494
	Standard error	0.2191	0.0363	0.0457	−
Model 2	Estimate	−4.1798	0.7152	−0.1390	0.2520
	Standard error	0.2333	0.0276	0.0463	−
Model 3	Estimate	−3.6049	1.1316	−0.1645	0.2517
	Standard error	0.2110	0.0436	0.0459	−
Model 2′	Estimate	−3.0977	0.8044	−0.1291	0.2631
	Standard error	0.2019	0.0327	0.0486	−
Model 3′	Estimate	−4.2507	1.0235	−0.1759	0.2560
	Standard error	0.2406	0.0403	0.0466	−

Table 6. Log-likelihood ($\mathcal{L}$) and Akaike information criterion (AIC) of the preferred and alternative models

Model	$\mathcal{L}$	AIC
Model 1, fixed slope (preferred model)	14.49	−22.99
Model 3′, fixed slope (alternative model)	12.05	−18.10

Table 7. Rupture length preferred and alternative model coefficients

Model	Coefficient	c_0	c_1	c_2	$\sigma_{SRL-unb}$
Model 1, fixed slope	Estimate	−4.1728	1	−0.1287	0.2503
(preferred model)	Standard error	0.0242	—	0.0425	—
Model 3′, fixed slope	Estimate	−4.1113	1	−0.1855	0.2553
(alternative model)	Standard error	0.0248	—	0.0434	—

to a $\sim\sqrt{W}$ scaling for width-limited events. The SCEC simulations show some extra support for $\sim\sqrt{A}$ scaling. While a limited width (15 and 19 km) is set for all simulations, the smooth transition near the limited width and deeper scattering width for larger earthquakes indicate that a fixed limited width is not suitable for the general scaling. As shown in simulations of Wang and Goulet (2022), the deep penetration of large earthquakes keeps increasing average displacements with the rupture length approaching a $\sqrt{A}$ scaling. In addition, Thingbaijam et al. (2017) observed $D \sim A^{0.429 \pm 0.134}$ for reverse events, $D \sim A^{0.858 \pm 0.214}$ for normal events, and $D \sim A^{0.597 \pm 0.112}$ for strike-slip events, which also support a $\sqrt{A}$ scaling for reverse and strike-slip events, while for normal events a relationship that is in between linear and square-root scaling. In hazard calculations, the square-root dependence has been applied as one of the logic stress dealing with epistemic uncertainties in the Uniform California Earthquake Rupture Forecast version 3 (Field et al., 2015).

Figure 7 presents the median magnitude scaling for the preferred and alternative models for strike-slip events for a seismological zone thickness equal to 15 and 20 km against the empirical data for the same fault type and seismological zone thickness up to 25 km. For the 15 km thick zone, the magnitude break occurs at **M**6.9. For the 20 km crust, a larger rupture area is needed for the event to become width-limited; thus, the magnitude break occurs closer to **M**7.3. The change in magnitude scaling is more significant in the preferred model than in the alternative model. The empirical data show consistent trends; at small magnitudes, there is no systematic difference between events in thin and thick parts of the seismogenic zones, while at larger magnitudes, there is a positive shift for events in thin parts of the seismogenic zone compared to events on thicker seismogenic zones.
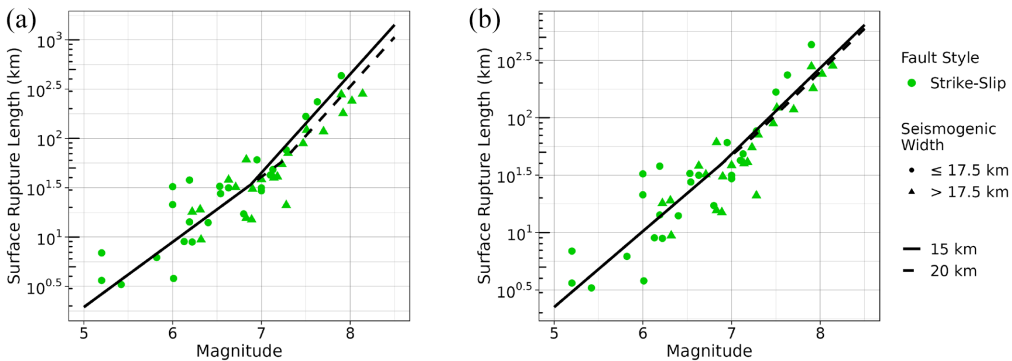

Figure 7. Magnitude scaling of the preferred model (a) and alternative model (b) for strike-slip events with a 15 km thickness of seismogenic zone, shown with the solid line, and a 20 km thickness of seismogenic zone, shown with the dashed line. Circular markers correspond to strike-slip events on seismological zones less than 17.5 km thick, and triangular markers correspond to strike-slip events on seismological zones between 17.5 and 25 km thick.
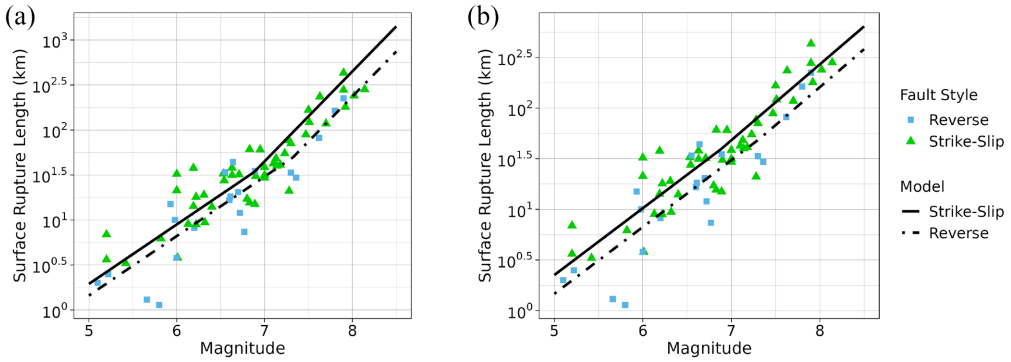
Figure 8. Magnitude scaling of the preferred model (a) and alternative model (b) for strike-slip events shown with the solid line, and reverse-slip events shown with the dash-dotted line. Both cases were evaluated for a seismological zone thickness of 15 km. The empirical data for strike-slip events on seismogenic zones up to 25 km are also depicted; triangular markers correspond to strike-slip events and square markers correspond to reverse events.

Figure 8 shows the preferred and alternative model scaling for strike-slip and reverse-slip events for a seismological zone thickness equal to 15 km. The vertical offset between the two models is introduced by the F_D term, and the difference in the magnitude break is caused by the different dip angles between strike-slip and reverse faults. Although the same seismological thickness was assumed for both fault styles, the shallower dip angle of reverse faults allows for a wider fault width which can accommodate larger events before they become width-limited. The preferred model captures the style of faulting effects primarily through the break in magnitude scaling suggesting that they are more noticeable at large magnitudes, while the alternative model captures the style of faulting effects primarily through the additive term suggesting they are similar for small-to-moderate and large events. The magnitude break for the strike-slip events occurs at **M**6.9 and for reverse events at **M**7.3. Consistent trends are also observed in the empirical data.

Figure 9 compares the regression residuals from the W&C type model (model 0) with the residuals from the preferred and alternative models (models 1 and 3′ with fixed slopes). All models have similar zero-mean-centered residuals for unbounded ruptures. However, Figure 9a shows a positive bias in the W&C type model residuals for width-limited ruptures, whereas in Figure 9b and c the residuals for width-limited ruptures of the selected models are centered closer to zero. Furthermore, the width-limited residuals exhibit less bias in the preferred compared to the alternative model. This comparison illustrates the advantage of seismological-theory-based models; a quadratic functional form would address the positive bias for the residuals but it would provide no basis for its existence. Relating the change in magnitude scaling to the finite thickness of the seismogenic zone increases the confidence in an extrapolation behavior that is scientifically defensible.

Preliminary regressions showed a magnitude-dependent aleatory variability that is by a factor of two smaller for width-limited ruptures as compared to unbounded ruptures. A rupture width transition parameter (δ_W) is introduced, and defined as:

$$\delta_W = \log_{10}(W_{\text{unb}}) - \log_{10}(W_{\text{lim}}) = \beta_1 \mathbf{M} + \beta_2 - \log_{10}(W_{\text{lim}}) \qquad (24)$$
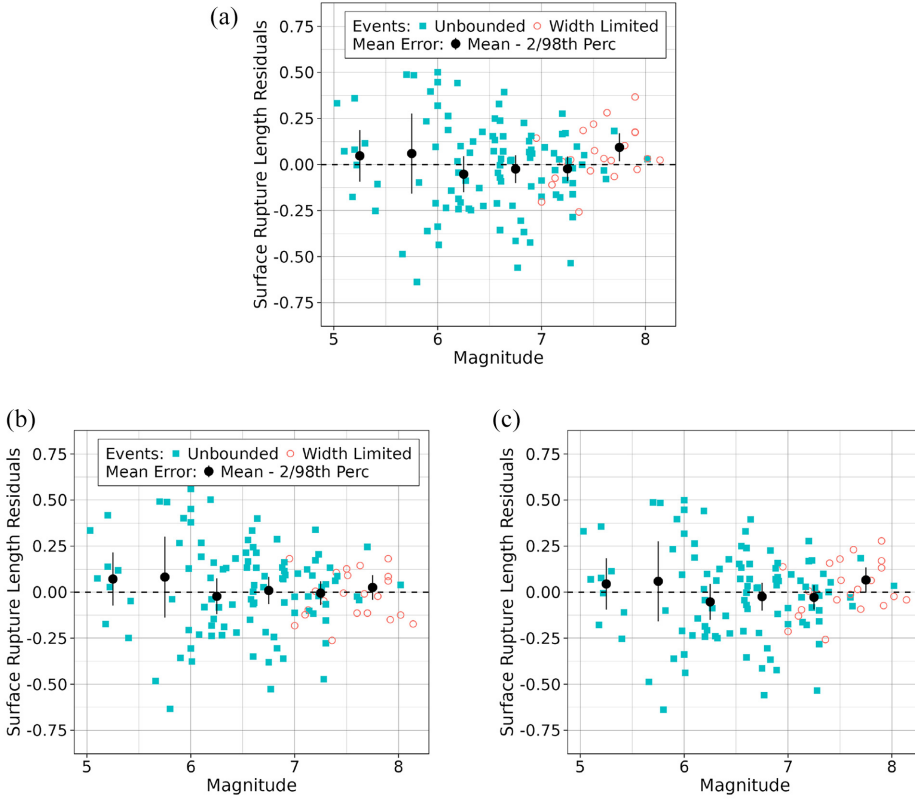
Figure 9. Comparison of regression residuals versus magnitude for (a) the W&C type model (model 0), (b) preferred model (model 1 with fixed slope), and (c) alternative model (model 3′ with fixed slope). The solid markers correspond to the unbounded events, while the open markers correspond to the width-limited events. The error bars indicate the 2nd, mean, and 98th percentile of the standard error of the mean of the binned residuals.

where W_{unb} is the theoretical rupture width for an infinite thickness seismological zone estimated from the first leg of rupture width model from Equation 3 ($\log_{10}(W_{unb}) = \beta_1 \mathbf{M} + \beta_2$) with the estimated coefficients in Table 3. A negative δ_W indicates an unbounded rupture, while a positive δ_W indicates a width-limited rupture, with the transition occurring around zero. Using the parameter δ_W, a heteroscedastic standard deviation model for the aleatory variability is proposed ($\epsilon_{SRL} \sim \mathcal{N}(0, \sigma_{SRL}(\delta_W))$) that gradually shifts from unbounded to width-limited ruptures based on a sigmoid function:

$$\sigma_{SRL}(\delta_W) = \frac{\sigma_{SRL-unb}}{1 + S(10 \ln(9)\delta_W)} \tag{25}$$

where σ_{SRL} is the magnitude-dependent standard deviation, and $\sigma_{SRL-unb}$ is the standard deviation for unbounded ruptures reported in Table 7. The sigmoid function is defined as ($S(x) = 1/(1 + \exp(-x))$). Figure 10 presents the regression residuals and proposed standard deviation versus the parameter δ_W for the preferred and alternative models. The factor $10 \times \ln(9)$ is used so that 80% of the standard deviation change occurs between $\delta_W = -0.1$ and 0.1, which is consistent with the empirical observations.
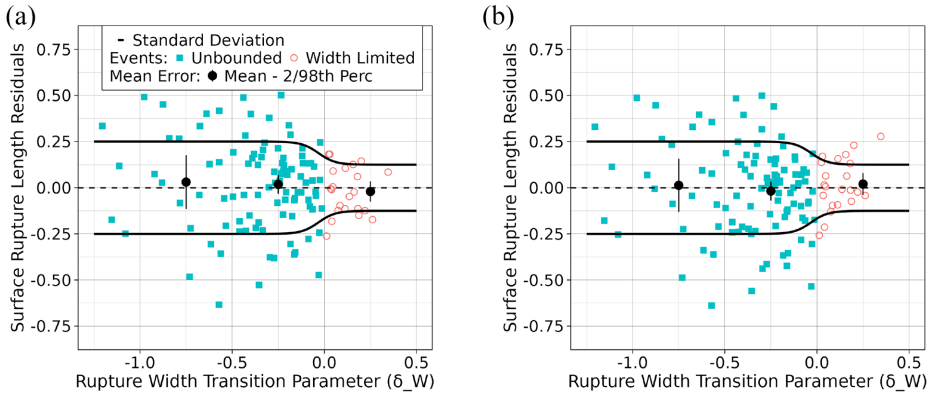
Figure 10. Proposed magnitude-dependent aleatory standard deviation and regression residuals versus the rupture width transition parameter (δ_W) for the preferred (a) and alternative (b) model.

Comparison with existing relationships

A series of comparisons with available models was performed to ensure the reasonableness of the proposed relationships. Figure 11 compares the preferred and alternative models with existing SRL relationships. "WC94 All," "WC94 SS," and "WC94 N" correspond to the Wells and Coppersmith (1994) SRL~$\mathbf{M}$ scaling relationships for all, strike-slip, and normal events; the scaling relationship for reverse events is omitted due to low significance levels. "W08 All," "W08 SS," and W08 R" are the Wesnousky (2008) SRL relationships for all, strike-slip, and reverse shallow-crustal events. The Wesnousky (2008) SRL relationship for normal events is not included in this comparison due to poor constraints. "L10 SS" and "L10 DS" correspond to the Leonard (2010) SRL~$\mathbf{M}$ relationships for dip-slip and strike-slip shallow-crustal events, while "L10 SCR" corresponds to stable continental regions. "L14 SCR DS" is the updated Leonard (2014) relationship for dip-slip events in stable continental regions. Finally, "WY15 OLS" and "WY15 Deming" correspond to the Wells and Youngs (2015) SRL~$\mathbf{M}$ relationships estimated with ordinary least squares and errors in variables regression methods.

The developed models are in overall agreement with the existing relationships over different magnitude ranges (Figure 11). In Figure 11a, the existing models for all and strike-slip events cover the range of both the preferred and alternative scaling relationships. The relationships from Wells and Coppersmith (1994) and Leonard (2010) are in better agreement with the proposed model at the small-to-moderate magnitude range. In contrast, Wesnousky (2008) and Wells and Youngs (2015) are in better agreement with the proposed relationships at the large magnitude range. For normal and reverse events in shallow-crustal environments (Figure 11b and c), the existing relationships overestimate the size of SRL for small-to-moderate magnitudes, while the proposed relationships predict larger SRL for large events. Leonard (2010) has a similar slope to the developed models, whereas Wells and Coppersmith (1994) and Wesnousky (2008) have a lower slope compared to the developed models. Finally, Figure 11d compares existing models for stable continental regions with the predictions of the proposed models, which were produced for dip-slip events, at a 30 km thick crust and a 60° fault angle. The proposed models have similar slopes to the existing relationships. Due to the increased thickness of the crust and shallow dip angle, the proposed relationships are predominately linear, with the magnitude break only occurring at very large magnitudes ($M>8$).
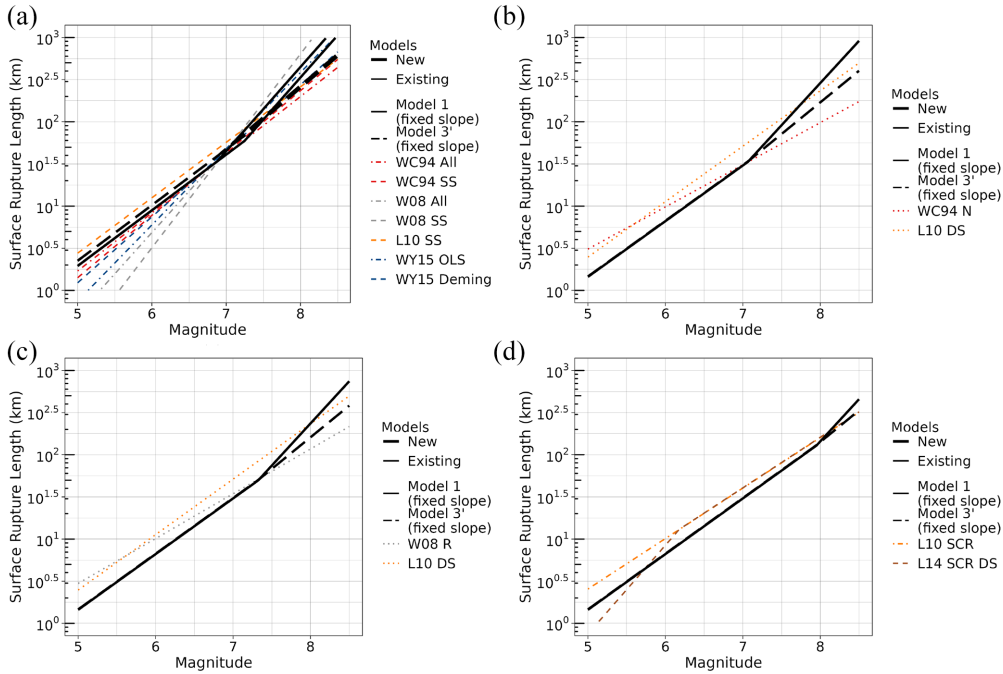
Figure 11. Comparison of the preferred (model 1 with fixed slope) and alternative (model 3′ with fixed slope) with existing SRL relationships. (a) Strike-slip faults on a 15 and 20 km thick crust, (b) normal faults on a 15 km thick crust, (c) reverse faults on a 15 km thick crust, and (d) normal faults on a 30 km thick crust.

Range of applicability

A **M**5 lower limit is recommended as it is the smallest magnitude in the regression data set. For the upper limit, the largest event in the data set was **M**8.1. However, the authors believe that seismological constraints will help the extrapolation up to **M**8.5, albeit with increased epistemic uncertainty.

Discussion and conclusions

The proposed SRL models capture the change in magnitude scaling between unbounded and width-limited ruptures through the use of seismological constraints and dynamic fault rupture simulations. Seismological theory was used to derive candidate scaling relationships between the moment magnitude (M), subsurface length (L), and rupture width (W). The dynamic rupture simulations constrained the $W \sim \mathbf{M}$ scaling. The empirical data were used to decide between the alternative scaling relationships for average displacement, to model the difference between L and SRL scaling, and to capture the aleatory variability in SRL scaling. The empirical data supports a $\sqrt{A}$-type scaling for the entire regime followed by the alternative model, which has a $\sqrt{A}$-type scaling for unbounded ruptures and transitions to L-type scaling for width-limited events. Other scaling relationships that were evaluated were pure W-type and L-type scaling, and composite relationship with $\sqrt{A}$ scaling for unbounded events that transition to W scaling for width-limited ruptures.

Compared to a simple linear regression between SRL and **M**, the proposed functional form provides a better fit to empirical data sets. Both the linear and the proposed functional forms have similar fits for unbounded ruptures, but the proposed relationship provides a better fit for width-limited events. A quadratic functional form could have been used to resolve the positive bias at large magnitudes, but it would lack a seismological basis limiting the confidence for its extrapolation. A width transition parameter, δ_W, is proposed to capture the difference in aleatory variability between unbounded and width-limited ruptures. The parameter δ_W corresponds to the log of the ratio of the theoretical rupture width for an infinitely thick seismogenic and the actual fault width. A comparison with existing SRL relationships showed consistent scaling with the proposed models for a range of fault types and tectonic environments.

Future studies should evaluate the effect of the thickness of the seismogenic zone using fault-specific information. In addition, a fully consistent scaling model for magnitude, rupture area, subsurface rupture length and width, and SRL for unbounded and width-limited ruptures using a more comprehensive data set following the presented framework is encouraged.

ORCID iDs

Grigorios Lavrentiadis ⓘ https://orcid.org/0000-0001-6546-1340

Yousef Bozorgnia https://orcid.org/0000-0003-1773-2489
Christine A Goulet https://orcid.org/0000-0002-7643-357X

Data and resources

The regression code and regression data sets are provided in: https://github.com/NHR3-UCLA/ LWABC23_SRL_model. The statistical regressions were performed using the computer software R and stats package (R Core Team, 2022). The open-source software package Support Operator Rupture Dynamics (SORD) can be downloaded from https://github.com/wangyf/sordw3.

References

Akaike H (1998) Information theory and an extension of the maximum likelihood principle. In: Parzen E, Tanabe K and Kitagawa G (eds) *Selected Papers of Hirotugu Akaike*. New York: Springer, pp. 199–213.

Baize S, Scotti O, Ritz J-F, Ferry M, Larroque C, Mathot E, Audin L, Nurminen F, Boncio P and Delouis B (2020) Surface ruptures during moderate earthquakes: Is that so rare? In: *Conference: GSA 2020 connects online*, Montreal, QC, Canada, 26–30 October.

Bodin P and Brune JN (1996) On the scaling of slip with rupture length for shallow strike-slip earthquakes: Quasi-static models and dynamic rupture propagation. *Bulletin of the Seismological Society of America* 86: 1292–1299.

Brune JN (1971) Correction to tectonic stress and the spectra of seismic shear waves from earthquakes. *Journal of Geophysical Research* 76: 1971.

Field EH, Biasi GP, Bird P, Dawson TE, Felzer KR, Jackson DD, Johnson KM, Jordan TH, Madden C, Michael AJ, Milner KR, Page MT, Parsons T, Powers PM, Shaw BE, Thatcher WR, Weldon RJ and Zeng YH (2015) Long-term time-dependent probabilities for the Third Uniform California Earthquake Rupture Forecast (UCERF3). *Bulletin of the Seismological Society of America* 105: 511–543.

Hanks TC and Bakun WH (2002) A bilinear source-scaling model for M-log A observations of continental earthquakes. *Bulletin of the Seismological Society of America* 92: 1841–1846.

Harris RA, Barall M, Aagaard B, Ma S, Roten D, Olsen K, Duan BC, Liu DY, Luo B, Bai KC, Ampuero JP, Kaneko Y, Gabriel AA, Duru K, Ulrich T, Wollherr S, Shi ZQ, Dunham E, Bydlon S, Zhang ZG, Chen XF, Somala SN, Pelties C, Tago J, Cruz-Atienza VM, Kozdon J, Daub E, Aslam K, Kase Y, Withers K and Dalguer L (2018) A suite of exercises for verifying dynamic earthquake rupture codes. *Seismological Research Letters* 89: 1146–1162.

Huang J-Y, Abrahamson NA, Chao S-H and Sung C-H (2023) New empirical source scaling laws for crustal earthquakes incorporating the fault dip angle and seismogenic thickness effects. [Unpublished Manuscript].

Ida Y (1972) Cohesive force across tip of a longitudinal-shear crack and Griffiths specific surface-energy. *Journal of Geophysical Research* 77: 3796–3805.

Kanamori H (1977) The energy release in great earthquakes. *Journal of Geophysical Research* 82: 2981–2987.

Lavrentiadis G and Abrahamson NA (2019) Generation of surface-slip profiles in the Wavenumber domain. *Bulletin of the Seismological Society of America* 109: 888–907.

Lavrentiadis G and Abrahamson NA (this issue) A local event coordinate system for surface fault rupture. *Earthquake Spectra*.

Leonard M (2010) Earthquake fault scaling: Self-consistent relating of rupture length, width, average displacement, and moment release. *Bulletin of the Seismological Society of America* 100: 1971–1988.

Leonard M (2014) Self-consistent earthquake fault-scaling relations: Update and extension to stable continental strike-slip faults. *Bulletin of the Seismological Society of America* 104: 2953–2965.

Mai PM and Beroza GC (2000) Source scaling properties from finite-fault-rupture models. *Bulletin of the Seismological Society of America* 90: 604–615.

Moss RES and Ross ZE (2011) Probabilistic fault displacement hazard analysis for reverse faults. *Bulletin of the Seismological Society of America* 101: 1542–1553.

Pegler G and Das S (1996) Analysis of the relationship between seismic moment and fault length for large crustal strike-slip earthquakes between 1977–92. *Geophysical Research Letters* 23: 905–908.

Petersen MD, Dawson TE, Chen R, Cao T, Wills CJ, Schwartz DP and Frankel AD (2011) Fault displacement hazard for strike-slip faults. *Bulletin of the Seismological Society of America* 101: 805–825.

R Core Team (2022) *R: A Language and Environment for Statistical Computing*. Vienna: R Foundation for Statistical Computing.

Romanowicz B (1992) Strike-slip earthquakes on quasi-vertical transcurrent faults: Inferences for general scaling relations. *Geophysical Research Letters* 19: 481–484.

Romanowicz B (1994) Comment on "A reappraisal of large earthquake scaling" by C. Scholz. *Bulletin of the Seismological Society of America* 84: 1675–1676.

Romanowicz B and Rundle JB (1993) On scaling relations for large earthquakes. *Bulletin of the Seismological Society of America* 83: 1294–1297.

Sarmiento A, Madugo D, Bozorgnia Y, Shen A, Mazzoni S, Lavrentiadis G, Dawson T, Madugo C, Kottke A, Thompson S, Baize S, Milliner C, Nurminen F, Boncio P and Visini F (2022) *Fault displacement hazard initiative database*. Technical Report, Report GIRS-2021-08. Los Angeles, CA: UCLA Natural Hazards Risk and Resiliency Research Center.

Scholz CH (1982) Scaling laws for large earthquakes: Consequences for physical models. *Bulletin of the Seismological Society of America* 72: 1–14.

Scholz CH (1994) A reappraisal of large earthquake scaling. *Bulletin of the Seismological Society of America* 84: 215–218.

Scholz CH (1997) Size distributions for large and small earthquakes. *Bulletin of the Seismological Society of America* 87: 1074–1077.

Scholz CH (1998) A further note on earthquake size distributions. *Bulletin of the Seismological Society of America* 88: 1325–1326.

Thingbaijam KKS, Mai PM and Goda K (2017) New empirical earthquake source-scaling laws. *Bulletin of the Seismological Society of America* 107: 2225–2246.

Wang Y and Day SM (2017) Seismic source spectral properties of crack-like and pulse-like modes of dynamic rupture. *Journal of Geophysical Research-solid Earth* 122: 6657–6684.

Wang Y and Day SM (2020) Effects of off-fault inelasticity on near-fault directivity pulses. *Journal of Geophysical Research: Solid Earth* 125: e2019JB019074.

Wang Y and Goulet C (2021) Validation of fault displacements from dynamic rupture simulations against the observations from the 1992 Landers earthquake. *Bulletin of the Seismological Society of America* 111: 2574–2594.

Wang Y and Goulet C (2022) Constraining fault displacements for strike-slip events using physics-based simulations. In: *The 12th national conference on earthquake engineering*, Salt Lake City, UT, 27 June–1 July.

Wells DL and Coppersmith KJ (1994) New empirical relationships among magnitude, rupture length, rupture. *Bulletin of the Seismological Society of America* 84: 974–1002.

Wells DL and Youngs R (2015) Improved regression relations for earthquake source parameters. In: *SSA 2015 annual meeting*, Pasadena, CA, 21–23 April.

Wesnousky SG (2008) Displacement and geometrical characteristics of earthquake surface ruptures: Issues and implications for seismic-hazard analysis and the process of earthquake rupture. *Bulletin of the Seismological Society of America* 98: 1609–1632.

Youngs RR, Arabasz WJ, Anderson RE, Ramelli AR, Ake JP, Slemmons DB, McCalpin JP, Doser DI, Fridrich CJ, Swan FH, Rogers AM, Yount JC, Anderson LW, Smith KD, Bruhn RL, Knuepfer PLK, Smith RB, DePolo CM, O'Leary DW, Coppersmith KJ, Pezzopane SK, Schwartz DP, Whitney JW, Olig SS and Toro GR (2003) A methodology for probabilistic fault displacement hazard analysis (PFDHA). *Earthquake Spectra* 19: 191–219.